Title
Dynamic Characterization of Thin Film Magnetic Materials

Author
GU, WEI

Publication Date
2016

Peer reviewed|Thesis/dissertation

UNIVERSITY OF CALIFORNIA

Los Angeles

Dynamic Characterization of Thin Film Magnetic Materials

A thesis submitted in partial satisfaction

of the requirements for the degree Master of Science

in Electrical Engineering

by

Wei Gu

2016

ABSTRACT OF THE THESIS

Dynamic Characterization of Thin Film Magnetic Materials

By

Wei Gu

Master of Science in Electrical Engineering

University of California, Los Angeles, 2016

Professor Yuanxun Wang, Chair

A broadband dynamic method for characterizing thin film magnetic material is presented. The method is designed to extract the permeability and linewidth of thin magnetic films from measuring the reflection coefficient (S11) of a house-made and short-circuited strip line testing fixture with or without samples loaded. An adaptive de-embedding method is applied to remove the parasitic noise of the housing. The measurements were carried out with frequency up to 10GHz and biasing magnetic fields up to 600 Gauss. Particular measurement setup and 3-step experimental procedures are described in detail. The complex permeability of a 330nm thick continuous FeGaB, 435nm thick laminated FeGaB film and a 100nm thick NiFe film will be induced dynamically in frequency-biasing magnetic field spectra and compared with a theoretical model based on Landau-Lifshitz-Gilbert (LLG) equations and eddy current theories. The ferromagnetic resonance (FMR) phenomenon can be observed among these three magnetic materials investigated in this thesis.

The thesis of Wei Gu is approved.

Tatsuo Itoh

Yahya Rahmat-Samii

Yuanxun Wang, Committee Chair

University of California, Los Angeles

2016

TABLE OF CONTENTS

LIST OF FIGURES

CHAPTER 1

Introduction

1.1 Motivation

The conventional conformal antennas suffer from poor radiation efficiency and excessive storage of reactive energy due to platform effects and high sensitivity of Ohmic loss. And the size of the conventional antenna is also constrained by operating frequency. It is imperative to design electrically small and low profile antennas with high performance to overcome those shortages which conventional antennas possessed. Strain mediated multi-ferroic antennas, represented by surface acoustic wave (SAW) and bulk acoustic wave (BAW) antennas, can be potentially the new generation of antennas. One proposed structure of BAW antenna is shown here [7]:

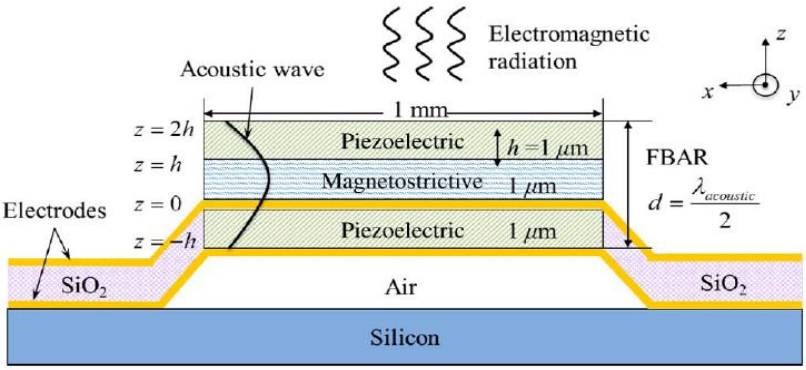

Fig. 1.1 The structure of BAW-resonance-based antenna

BAW antennas use dynamic electric or magnetic flux as radiation source instead of conductive current, which promise the extinction of the Ohmic loss. Using magnetic flux as radiation source can also benefit improving BAW antennas' radiation performance by reducing the platform effect and rising the radiation efficiency. Because this time the image effect will enhance the radiation of the magnetic flux not cancel it. In order for BAW antenna to achieve low observability, it should be built with thin film magnetic material with high permeability and high permittivity simultaneously. Additionally, magnetic materials with high permeability will also help to reduce the radiation quality factor of BAW antenna [7]. The equations below quantify exactly how much the high permeability is able to improve the radiation efficiency by lower the radiation quality factor of BAW antenna:

$$Q_{bound} = \omega \frac{W_{me}}{P_{rad}} = \omega \frac{{}^{W_H}\!/_{k_H^2}}{P_{rad}} = \frac{1}{k_H^2} \frac{1}{\mu_r k_0 h} \tag{1.1}$$

, where Q_{bound} indicates the lower bound of the radiation quality factor. k_0 is the free-space wave number and h is the thickness of the layer of magnetostrictive material shown in the Figure 1.1. k_H^2 is the maximum ratio of mechanical energy W_{me} transferred to the magnetic energy W_H in the form of magnetic flux density B. Mechanical energy carried by the acoustic wave is stored in the magnetostriction layer as indicated in the Figure 1.1. W_H and P_{rad} are calculated by the following equations:

$$P_{rad} = \frac{1}{2\eta_0} \iint |E_0|^2 ds \tag{1.2}$$

$$W_H = \iiint \frac{|B|^2}{\mu_T} dv \tag{1.3}$$

From equation 1.1, μ_r is a term of denominator, which indicates the higher the relative permeability the thin film has, the lower radiation quality factor the BAW antenna will possess.

So characterizing permeability of the thin film magnetic material becomes high priority to design BAW antenna. However, most of the existing approaches for permeability characterization of thin film magnetic materials are either not reliable for frequency above 1GHz or too complex to process the measurement data[8]. Therefore, an easy and precise approach is demanded to be developed for permeability and linewidth extraction.

1.2 Two Existing Permeability Measurement Techniques

1.2.1 The Coil Technique

The coil technique are proved to be efficient and appropriate in MHz frequency range and has been widely used in the past years. The magnetic biasing field for the coil technique has to be generated by an external drive coil. The permeability of the testing sample can be extracted from the difference between the impedances of the coil with and without the sample inside.[3][5][6] However, the dimensional resonance and conductivity effects due to the relative big size of the coil cut down the sensitivity of the technique at higher band frequencies than MHz frequencies.

1.2.2 The Two Port Coaxial Transmission Line Technique

Two-port coaxial transmission line method [8] is another typical method developed these days to measure permeability especially in GHz frequency range. However, this technique is limited to

flexible ferromagnetic materials and very restrictive for sample preparation. It doesn't conform to the specification of an easy operational technique.

1.3 A Better Dynamic Solution: One Port Strip line Measurements

Compared to the coil technique which is not reliable or accurate in GHz frequency range and two-port measurement technique with complex setup procedure, one-port strip line method is a perfect fit for high frequency permeability extraction. The traditional one-port transmission line technique [1] [2] can only measure the in-plane complex permeability of thin films regarding frequency spectra with a static magnetic biasing field added. The linewidth of the thin film material cannot be obtained directly from the measurements.

In this paper, the one-port strip line technique is improved by applying dynamic magnetic biasing fields to the measurements. The permeability will be measured in terms of frequency and biasing magnetic field simultaneously. The linewidth can be read plainly from the plot where the permeability at certain frequency is with respect to the biasing magnetic field.

The upgraded one-port strip line measurement was performed with a continuous FeGaB thin film, a laminated FeGaB thin film and a NiFe thin film inserted into the permeameter. The permeameter consists of a one port short-circuited strip line housing and a brass cover on top. Theoretical analysis based on LLG equations of these three thin films are given to predict FMR phenomenon and verify the correctness of the measurements.

CHAPTER 2

Operating Principle of the Strip Line Technique

2.1 Complex Permeability Extraction from Transmission Line Theory

According to the transmission line theory [4], the expressions of the incident voltage generated from the source at $z < 0$ on a lossy transmission line and the reflected wave caused by the load at the termination $(z = 0)$ of the transmission line can be defined as:

$$V(z)^{+} = V_0^{+} e^{-\gamma z} \tag{2.1a}$$

$$V(z)^{-} = V_0^{-} e^{\gamma z} \tag{2.1b}$$

, where V_0^{+} is the incident voltage amplitude at the loaded end and V_0^{-} is the reflected voltage amplitude at the terminated end. And γ is the complex propagation constant. The total voltage on the line is given by a sum of the incident and reflected waves:

$$\mathrm{V(z)} = V_0^{+} e^{-\gamma z} + V_0^{-} e^{\gamma z} \tag{2.2}$$

The voltage reflection coefficient R_0 is introduced by normalizing the amplitude of the reflected wave to the amplitude of the incident wave at the terminated end of the transmission line:

$$R_0 = \frac{V_0^-}{V_0^+} \tag{2.3}$$

So the reflection coefficient $R(l)$ of a short-circuit terminated lossy line at a distance l from the reference point, which is the terminated end, can be expressed as

$$R(l) = \frac{V_0^- e^{\gamma z}}{V_0^+ e^{-\gamma z}} = R_0 e^{-2\gamma l} \tag{2.4}$$

In this case, given the short-circuit end, R_0 is set as -1 and l denotes the length of the testing strip line. l can be separate into two parts, l_{sample} and l_{empty}. l_{sample} stands for the substrate length, while l_{empty} indicates the length of the empty strip line. $R(l)$ can be measured as S11 of the permeameter.

The expression of the complex propagation constant γ is determined by solving the wave equations in a general lossy medium. The wave equations result from Maxwell's curl equations by considering the effect of a lossy medium. If the medium is conductive, with a conductivity σ, the wave function for electric field $\bar{E}$ can be derived as below:

$$\nabla \times \bar{E} = -j\omega\mu\bar{H} \tag{2.5a}$$

$$\nabla \times \bar{H} = j\omega\varepsilon\bar{E} + \sigma\bar{E} \tag{2.5b}$$

Substitute (2.5b) into $\nabla \times$ (2.5a), which becomes:

$$\nabla^2\bar{E} + \omega^2\mu\left(\varepsilon - \frac{j\sigma}{\omega}\right)\bar{E} = 0 \tag{2.6}$$

Then,

$$\gamma = \sqrt{-\omega^2\mu(\varepsilon - \frac{j\sigma}{\omega})} = \frac{j\omega\sqrt{\mu_{eff}\varepsilon_{eff}}}{c_0} \tag{2.7}$$

, where $\omega = 2\pi f$. Since the thin film sample with substrate will be inserted into the strip line, which makes the whole system inhomogeneous, the propagation constant can also be defined in terms of effective permeability μ_{eff} and effective permittivity ε_{eff} by assuming the strip line as an effective homogeneous system based on quasi-transverse electromagnetic wave approximation. For Consistency,

$$\varepsilon_0\varepsilon_{eff} = \varepsilon - \frac{j\sigma}{\omega} \tag{2.8a}$$

$$\mu_0\mu_{eff} = \mu \tag{2.8b}$$

And,

$$c_0 = \frac{1}{\sqrt{\mu_0\varepsilon_0}} \tag{2.8c}$$

As soon as ε_{eff} is obtained from the measurements of S11, μ_{eff} can be calculated by solving the equations above. Applying the relationship between μ_r and μ_{eff} along with the distance h between the upper metal and ground plane of the strip line testing fixture and the thickness d of the thin film sample, the relative permeability μ_r can be described as:

$$\mu_r = \frac{\mu_{eff} - 1}{K(\frac{d}{h})} \tag{2.9}$$

, where K is the geometry dependent scaling factor, which should be chosen accordingly.

2.2 Complex Permeability Calculated Based on Ferromagnetic Component Theory

2.2.1 Constitution Relation with Magnetic Materials Presented

In free space, a simple relation hold between the magnetic field intensity $\bar{H}$ and flux density $\bar{B}$:

$$\bar{B} = \mu_0 \bar{H} \tag{2.10}$$

, where $\mu_0 = 4\pi \times 10^{-7}$ henry/m is the permeability of free space. This relation is commonly known as one of the constitution relations. However, if there are media presented other than free space, the total constitution relation above will be affected by the electromagnetic fields existing in the media. For a magnetic material, applying a magnetic biasing field H_0, a magnetic polarization or magnetization $\bar{M}$ which augments the total magnetic flux, $\bar{B}$, will be produced inside. Then we have the constitution relation as:

$$\bar{B} = \mu_0(\bar{M} + \bar{H}) \tag{2.11}$$

In the preceding discussion, $\bar{M}$ is a vector in the same direction as $\bar{H}$, which means it is assumed that the material is isotropic. For more general case, which means the anisotropic materials have been included, an even more complicated constitution relation has been characterized by a rank two permeability tensor, which is given in matrix form as:

$$\bar{B} = [\mu]\bar{H} \tag{2.12}$$

, which is extended as:

$$\begin{bmatrix} B_x \\ B_y \\ B_z \end{bmatrix} = \begin{bmatrix} \mu_{xx} & \mu_{xy} & \mu_{xz} \\ \mu_{yx} & \mu_{yy} & \mu_{yz} \\ \mu_{zx} & \mu_{zy} & \mu_{zz} \end{bmatrix} \begin{bmatrix} H_x \\ H_y \\ H_z \end{bmatrix} \tag{2.13}$$

2.2.2 The Single Spin Dynamic of the Electron

If the intensity of the biasing field increases till all the unbalanced electron spins are aligned, the material is considered to be magnetically saturated, while M_s indicates the saturation magnetization. In order to obtain the expression of $\bar{M}$ in terms of $\bar{H}$ under the condition that the material reaches magnetically saturation, the equation of motion for the magnetic dipole moments, which is the simplest form of LLG equation, needs to be derived based on the definition of torque exerted on the magnetic dipole and solved.

To derive the simplest form of the LLG equations, we start from the single spin dynamic of the electron inside the magnetic material [4]. The spin of an unbalanced electron creates the magnetic dipole moment which contributes to the magnetic properties of the interested material. The expression of the magnetic dipole moment $\bar{m}$ can be given as:

$$\bar{m} = \frac{q\bar{h}}{2m_e} \tag{2.14}$$

, where $\bar{h}$ is Planck's constant divided by 2π. q is the electron charge and m_e is the mass of the electron. And the expression of a spin angular momentum $\bar{s}$ can be written as:

$$\bar{s} = \frac{\bar{h}}{2} \tag{2.15}$$

From quantum mechanical perspective, the magnetic dipole moment of an electron $\bar{m}$ and its angular momentum $\bar{s}$ has a relationship written as follow:

$$\bar{m} = -r\bar{s} \tag{2.16}$$

, where r is gyromagnetic radio. Negative sign indicates that the magnetic dipole moment has an opposite direction to its angular momentum. Comparing (2.14) with (2.16) gives the following relation:

$$\gamma = \frac{q}{m_e} \tag{2.17}$$

Provided there are N unbalanced magnetic dipoles per unit volume, then the total magnetization contributes by these unbalanced electron spins can be calculated as:

$$\bar{M} = N\bar{m} \tag{2.18}$$

, and the torque $\bar{T}$ of a single spin equals to the first order derivative of angular momentum with respect to time, we have:

$$\bar{T} = \frac{d\bar{s}}{dt} \tag{2.19}$$

The torque $\bar{T}$ that impact on the magnetic dipole can also be described as:

$$\bar{T} = \mu_0\bar{m} \times \bar{H}_0 \tag{2.20}$$

Combine (2.19) and (2.20), we can easily build up the equation of motion for a single magnetic dipole moment as:

$$\frac{d\bar{s}}{dt} = \mu_0\bar{m} \times \bar{H}_0 \tag{2.21}$$

Based on the calculation of the total magnetization before, the equation of motion for a single magnetic dipole moments can be easily transferred to the equation of the motion for the total magnetization of the material, which is:

$$\frac{d\bar{M}}{dt} = -\mu_0 r\bar{M} \times \bar{H} \tag{2.22}$$

2.2.3 Tensor Permeability Analysis of Lossy Medium

When a small AC magnetic signal $\bar{H}$ interacts with the magnetically saturated material, total magnetization $\bar{M}$ and total field $\bar{H}$ can be decomposed as:

$$\bar{M}_t = M_s\hat{z} + \bar{M} \tag{2.23}$$

$$\bar{H}_t = H_0\hat{z} + \bar{H} \tag{2.24}$$

Assumed there is a time harmonic dependence e^{jwt} in the small AC signal, substitute (2.23), (2.24) into (2.22) then the first order differential equation will be further reduced to two ordinary phasor equations. Solving them, give us:

$$(\omega_0^2 - \omega^2)M_x = \omega_0\omega_m H_x + j\omega\omega_m H_y \tag{2.25}$$

$$(\omega_0^2 - \omega^2)M_y = -j\omega_0\omega_m H_x + \omega\omega_m H_y \tag{2.26}$$

$$\bar{M} = [\chi]\bar{H} = \begin{bmatrix} \chi_{xx} & \chi_{xy} & 0 \\ \chi_{yx} & \chi_{yy} & 0 \\ 0 & 0 & 0 \end{bmatrix}\bar{H} \tag{2.27}$$

, where $\omega_0 = \mu_0 r H_0$ and $\omega_m = \mu_0 r M_s$ are called $\mathcal{L}armor$ or $precession$ frequency. $[\chi]$ is denoted as the tensor susceptibility. Compared with the constitution relation, tensor permeability $[\mu]$ can be expressed as

$$[\mu] = \mu_0([U] + [\chi]) \tag{2.28}$$

Then the element of the tensor permeability is

$$\mu = \mu_0(1 + \chi_{xx}) = \mu_0\mu_r \tag{2.29}$$

, where $\chi_{xx} = \frac{\omega_0 \omega_m}{\omega_0^2 - \omega^2}$, which is given by turn the two ordinary phasor equations into its matrix form. For resonant system, equations to describe lossless system can be easily transfer to lossy ones by introducing a damping factor α, which makes both the $\mathcal{L}armor$ frequency and element of the tensor susceptibility complex:

$$\omega_0 \leftarrow \omega_0 + j\alpha\omega \tag{2.30}$$

$$\chi_{xx} \leftarrow \chi_{xx} = \chi'_{xx} - j\chi''_{xx} \tag{2.31}$$

The expressions of the real and imaginary part can be induced by substituting the complex $\mathcal{L}armor$ frequency into the original χ_{xx}, then we have:

$$\chi'_{xx} = \frac{\omega_0 \omega_m (\omega_0^2 - \omega^2) + \omega_0 \omega_m \omega^2 \alpha^2}{[\omega_0^2 - \omega^2(1+\alpha^2)]^2 + 4\omega_0^2 \omega^2 \alpha^2} \tag{2.32a}$$

$$\chi''_{xx} = \frac{\alpha\omega\omega_m[\omega_0^2 + \omega^2(1+\alpha^2)]}{[\omega_0^2 - \omega^2(1+\alpha^2)]^2 + 4\omega_0^2 \omega^2 \alpha^2} \tag{2.32b}$$

, where we approximate $1 + \alpha^2 \approx 1$. As for most magnetic material, the loss is small.

And the damping factor α can be determined by the linewidth ΔH of the complex susceptibilities:

$$\alpha = \frac{\Delta H \mu_0 r}{2\omega} \tag{2.33}$$

So the real and imaginary part of the complex relative permeability of the magnetic material can be obtained by:

$$\mu_r = \mu'_r + j\mu''_r \tag{2.34a}$$

$$\mu'_r = 1 + \chi'_{xx} \tag{2.34b}$$

$$\mu_r'' = -\chi_{xx}'' \tag{2.34c}$$

2.2.4 Kittel's Equation

In the previous derivation of tensor permeability, it is assumed that the DC magnetic bias field external to the thin film magnetic material is the same as internal. But practically, the magnetic field stimulated inside the sample is always different from the bias magnetic field outside due to the boundary conditions at the surface of the sample. In general, the shape of the magnetic material and the orientation of the DC bias field will decide the variation between the magnetic field inside and out. To quantify this distinction, the demagnetization factor $N = N_x, N_y \; or \; N_z$ for certain direction is introduced here. And N is defined to satisfy that $N_x + N_y + N_z = 1$. So the adjusted expression of the magnetic field inside $\overline{H}$ can be written as:

$$\overline{H} = \overline{H}_e - N\overline{M} \tag{2.35}$$

Expand equation (2.35) in the Cartesian coordinate system:

$$H_x = H_{xe} - N_x M_x \tag{2.36a}$$

$$H_y = H_{ye} - N_y M_y \tag{2.36b}$$

$$H_z = H_{ze} - N_z M_z \tag{2.36c}$$

Substitute (2.36a-c) into equation (2.27) to eliminate H_x and H_y and solve for M_x and M_y:

$$M_x = \frac{\chi_{xx}(1+\chi_{yy}N_y)-\chi_{xy}\chi_{yx}N_y}{D} H_{xe} + \frac{\chi_{xy}}{D} H_{ye} \tag{2.37a}$$

$$M_y = \frac{\chi_{yy}(1+\chi_{xx}N_x)-\chi_{xy}\chi_{yx}N_x}{D} H_{ye} + \frac{\chi_{yx}}{D} H_{xe} \tag{2.37b}$$

, where

$$D = (1 + \chi_{xx}N_x)(1 + \chi_{yy}N_y) - \chi_{yx}\chi_{xy}N_xN_y \tag{2.38}$$

For a finite magnetic material, at the gyromagnetic resonance frequency ω_r, D is set as 0. Substitute the expression of the element of tensor susceptibility into equation (2.38), which gives:

$$\left(1 + \frac{\omega_0\omega_m N_x}{\omega_0^2 - \omega^2}\right)\left(1 + \frac{\omega_0\omega_m N_y}{\omega_0^2 - \omega^2}\right) - \frac{\omega^2\omega_m^2}{(\omega_0^2 - \omega^2)^2}N_xN_y = 0 \tag{2.39}$$

Solve for ω, then we get the Kittel's equation as:

$$\omega_r = \omega = \sqrt{(\omega_0 + \omega_m N_x)(\omega_0 + \omega_m N_y)} \tag{2.40}$$

In the one port strip line measurement, the biasing field H_a is applied tangentially to the surface of the thin film along z direction. The direction perpendicular to the surface of the thin film magnetic material is set as y direction. As shown in the Figure 2.1. H_0 is the internal biasing field inside the thin film sample. According to the coordination of the thin film, we set $N_x = N_z = 0$ and $N_y = 1$, then we have:

$$\omega_r = \omega = \sqrt{\omega_0(\omega_0 + \omega_m)} \tag{2.41}$$

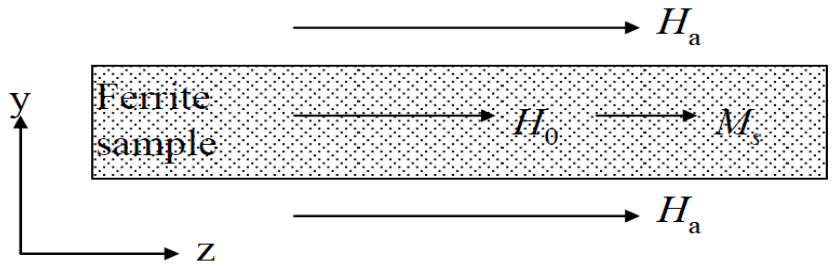

Figure 2.1 Tangential biased internal and external field for a thin film sample

2.2.5 Derivation of the Complete Form of χ_{xx} Tensor Susceptibility Element

Note that after the demagnetization factor is introduced, it is also necessary to rewrite the expression of χ_{xx}. The new χ_{xx} can be derived from equation (2.37a):

$$\chi_{xx\_de} = \frac{\chi_{xx}(1+\chi_{xx})+\chi_{xy}^2}{1+\chi_{xx}} \tag{2.42}$$

$$\chi_{xx\_de} = \frac{\omega_m(\omega_0+\omega_m)}{\omega_0(\omega_m+\omega_0)-\omega^2} \tag{2.43}$$

Now considering the effect of damping factor, we substitute equation (2.30) into (2.43):

$$\chi'_{xx\_de} = \frac{\omega_m\omega_0(\omega_m+\omega_0)^2-\omega^2\omega_m(\omega_m+\omega_0)+\alpha^2\omega^2\omega_m\omega_0}{[\omega_0^2+\omega_0\omega_m-(1+\alpha^2)\omega^2]^2+\alpha\omega^2(2\omega_0+\omega_m)^2} \tag{2.44a}$$

$$\chi''_{xx\_de} = \frac{\alpha\omega\omega_m[(\omega_m+\omega_0)^2+(1+\alpha^2)\omega^2]}{[\omega_0^2+\omega_0\omega_m-(1+\alpha^2)\omega^2]^2+\alpha\omega^2(2\omega_0+\omega_m)^2} \tag{2.44b}$$

(2.44a) and (2.44b) can be further simplified regarding FMR, which means Kittel's equation can be implemented here:

$$\chi'_{xx\_de} = \frac{\omega_m\omega_0\omega_r^2}{(\omega_0^2+\alpha^2\omega^2)(\omega_r^2-\omega^2)} \tag{2.45a}$$

$$\chi''_{xx\_de} = \frac{\alpha\omega\omega_m\omega_r^2}{(\omega_0^2+\alpha^2\omega^2)(\omega_r^2-\omega^2)} \tag{2.45b}$$

, which consist of the complete form of χ_{xx} with loss due to damping effect and demagnetization under consideration.

CHAPTER 3

Setup and Experimental Procedures of Measurements

3.1 Measurement Setup

The whole measurement system consists of a system DC power supply, an electromagnet, a vector network analyzer (VNA), a relay, a Gauss meter and a house made strip line testbed.

3.1.1 System DC Power Supply Setup

The system DC power supply is connected to the electromagnet. The output of the power supply is controlled by the computer to adjust the intensity of the magnetic field that the electromagnet produce. The maximum current of the DC power supply is set as 5A, which corresponds to the maximum biasing field that the electromagnet can provide, 625 Gauss. Sweep the scale of the biasing field with 200 sampling points.

3.1.2 Vector Network Analyzer Setup

The sweep frequency range of the VNA is set starting from 50MHz to 10GHz. The sampling points of the frequency amounts to 1601 points. The output power of the RF signal delivered by the VNA is ought to be low, however, it is highly possible that the high power RF signal induces the anisotropy of the material. The frequency of the small AC signal produced by the VNA is

1GHz. VNA, system DC power supply and the computer are connected to each other with GPIBs.

3.1.3 The Relay Setup

The relay is also managed by the computer for reversing the direction of the biasing magnetic field during the initialization of the measurements to eliminate the remnants on the electromagnet. The relay is also driven by an external DC power Supply.

3.1.4 The Gauss Meter Setup

The probe of the Gauss meter is placed at the center of the electromagnet. The data of the meter is read by computer through an ADC. The Gauss meter needs to be calibrated before it is located nearby the electromagnet.

3.1.5 The Sample Preparation

Before the measurements are implemented, a 330nm thick continuous FeGaB thin film, a 435 nm thick circular FeGaB thin film of 3mm diameter and a 100nm thick NiFe thin film should be deposited on 5mm*6mm*0.5mm silicon substrates. The circular thin film FeGaB sample is laminated, which means that one 37nm thick Al_2O_3 lamination is deposited in every two 18nm thick FeGaB laminations. Then 8 Al_2O_3 laminations and 8 FeGaB laminations are stacked together on the substrate.

3.1.6 The One Port Strip Line Permeameter

The strip line is designed to match to 50Ω. The total length of the strip line is 9mm. Since 9mm is shorter than a quarter wavelength at 10GHz, the strip line is appropriate to measurements at all

frequencies under 10GHz without having resonance effects. The distance between the upper line and the ground plate is 1mm. The width of the upper line is 4.9mm. In order to locate the thin film sample half way between the upper medal and ground, the thin film needs to be deposited on a 0.5mm thick Si substrate before inserted into the testbed. The thin film sample is placed close to the short-circuit end of the strip line to keep the magnetic field approximately uniform. The testbed is equipped with a brass housing to protect the strip line from external electric field interference. Figure 3.1 shows the appearance of the house made strip line testing fixture.

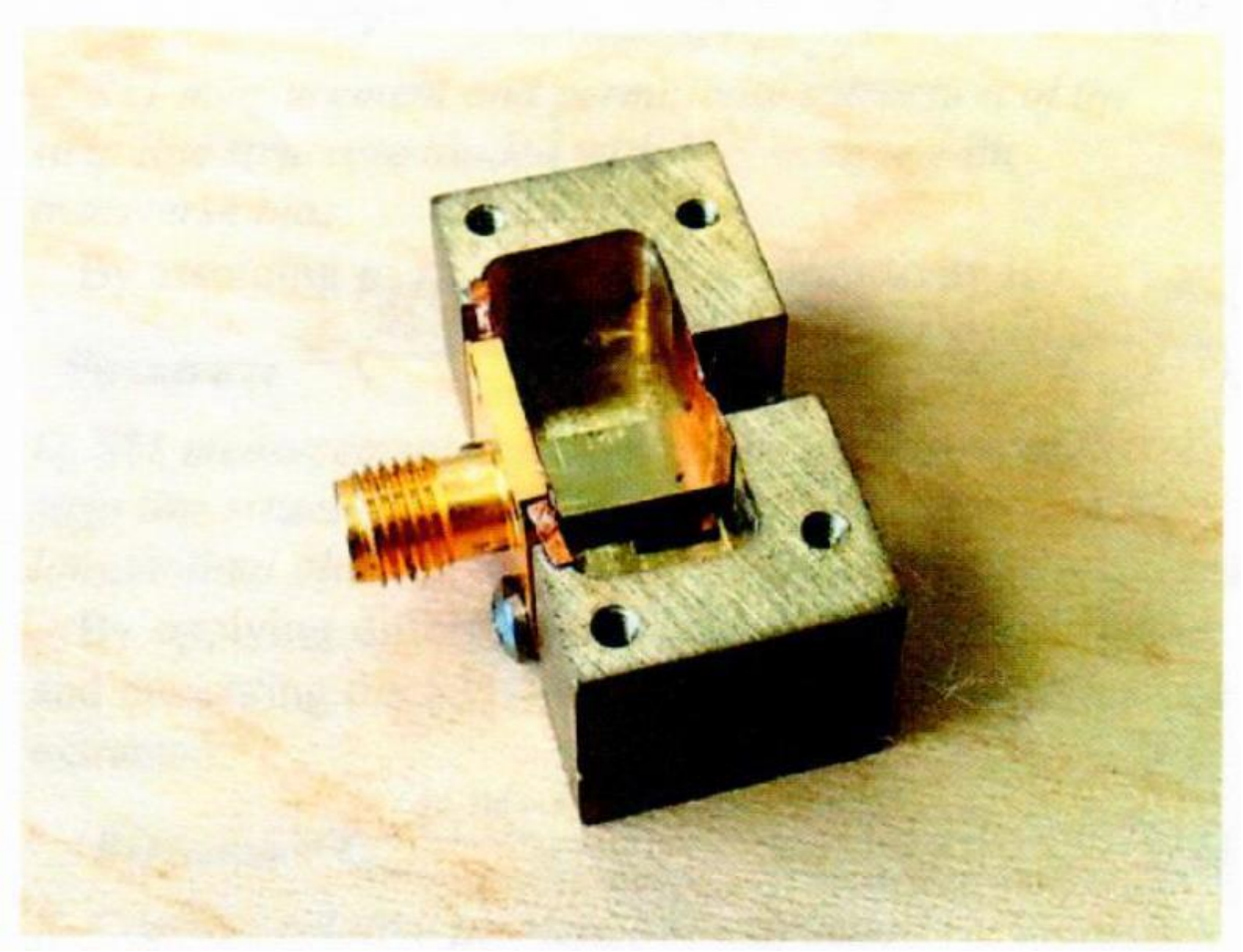

Fig. 3.1 One port permeameter based on short-circuited strip line housing

3.2 3-Step Experimental and Permeability Extraction Procedures

Initialize the VNA with the standard open, short and load calibration until the housing noise is lower than 0.05 dB. Calibrate the Gauss meter to zero when the output of the system DC power supply is zero.

3.2.1 Effective Permittivity of Empty Housing

Measure S_{11}^{empty} of the empty strip line with transverse and longitudinal magnetic biasing field applied respectively, $S_{11}^{empty\_T}$ and $S_{11}^{empty\_L}$. Assuming $\mu_{eff} = 1$, extract the effective permittivity $\varepsilon_{eff}^{empty}$ of the test environment with the frequency dependent conducting loss, dielectric loss and other parasitic noise of the housing included according to:

$$\varepsilon_{eff}^{empty} = \left(\frac{jc_0 \ln(S_{11}^{empty})}{2\omega l}\right)^2 \tag{3.1}$$

, where c_0 is the speed of light in free space.

3.2.2 Effective Permittivity with Substrate Inside

Insert the thin film sample into the strip line. Measure S_{11}^{sub} of the loaded strip line with only transverse magnetic biasing field added. The effective permeability sustains as 1. Extract the effective permittivity ε_{eff}^{sub} with the influence of the substrate considered based on:

$$\varepsilon_{eff}^{sub} = \left(\frac{jc_0 \ln(-S_{11}^{sub})}{2\omega l_{sample}} - \frac{\sqrt{\varepsilon_{eff}^{empty}} l_{empty}}{l_{sample}}\right)^2 \tag{3.2}$$

3.2.3 Effective Permeability with Thin Film Sample Loaded

Measure S_{11}^{f} of the loaded strip line with longitudinal magnetic biasing field. Extract the effective permeability μ_{eff} of the magnetic material de-embedded by $\varepsilon_{eff}^{empty}$ and ε_{eff}^{sub}:

$$\mu_{eff} = \left(\frac{jc_0 \ln(-S_{11}^{f})}{2\omega l_{sample}\sqrt{\varepsilon_{eff}^{sub}}} - \frac{\sqrt{\varepsilon_{eff}^{empty}}\, l_{empty}}{\sqrt{\varepsilon_{eff}^{sub}}\, l_{sample}} \right)^2 \tag{3.3}$$

Using the relationship between μ_r and μ_{eff} mentioned before in Operating Principle, μ_r can be calculated.

3.2.4 De-embedding to S11

Note that every time when changing the direction of the biasing field from transverse side to longitudinal one, the calibration of the VNA needs to be done again. When calculating the effective permeability, further de-embedding method to S11 is performed:

$$\left|S_{11}^{empty}\right| \leftarrow \left|S_{11}^{empty\_T}\right| - \left|S_{11}^{empty\_T}\right| \tag{3.4a}$$

$$\left|S_{11}^{sub}\right| \leftarrow \left|S_{11}^{sub}\right| - \left|S_{11}^{empty\_T}\right| \tag{3.4b}$$

$$\left|S_{11}^{f}\right| \leftarrow \left|S_{11}^{f}\right| - \left|S_{11}^{empty\_L}\right| \tag{3.4c}$$

CHAPTER 4

Dynamic Characterizations of Three Different Magnetic Materials

4.1 Continuous FeGaB

Figure 4.1 and Figure 4.2 show the real part and imaginary part of the relative permeability in frequency-field spectra extracted from the measurements of continuous FeGaB. FMR can be observed in both parts of the complex relative permeability. And resonance frequency moves from the lower band to the higher band, as the strength of the magnetic biasing field increases.

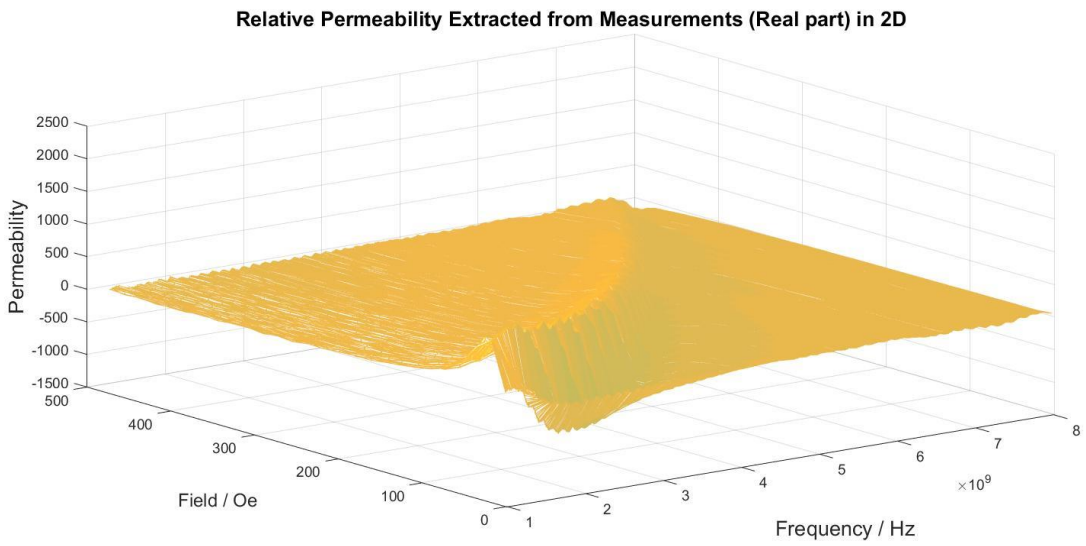

Fig. 4.1 μ_r' of continuous FeGaB in the field-frequency spectra

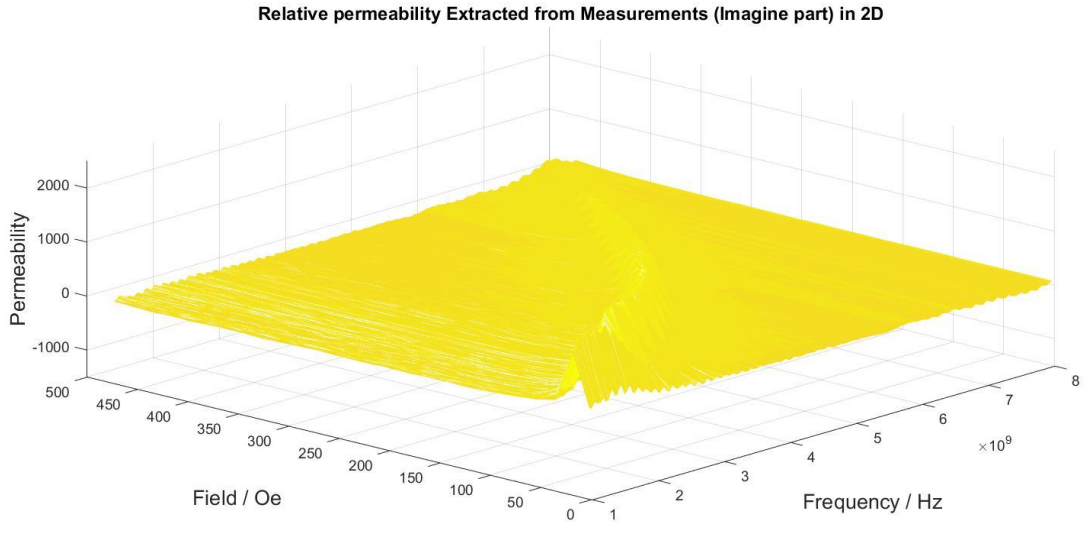

Fig. 4.2 μ_r'' of continuous FeGaB in the field-frequency spectra

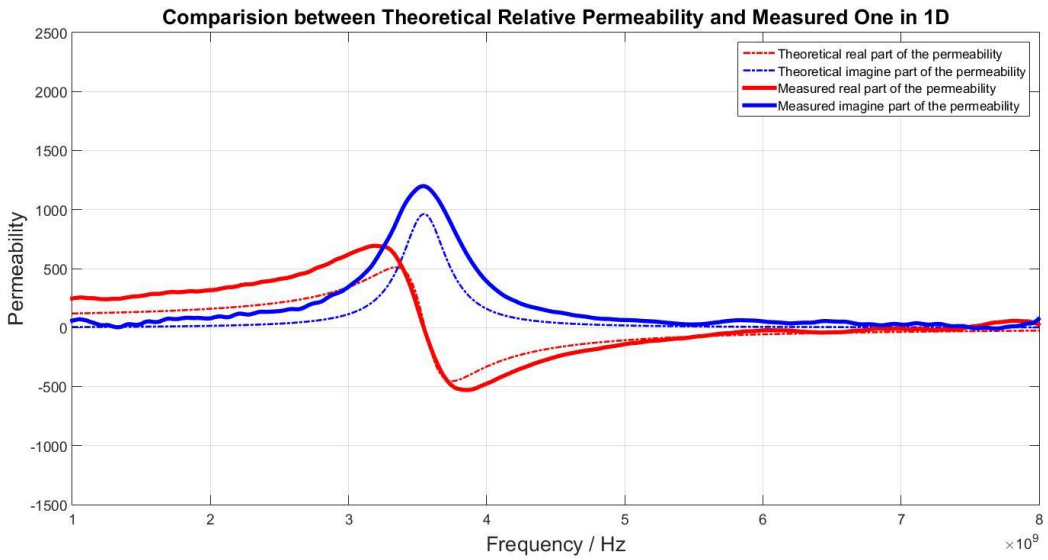

Fig. 4.3 μ_r' and μ_r'' of continuous FeGaB in frequency spectra compared with theoretical results

Figure 4.3 shows the complex permeability in only frequency spectra at certain magnetic biasing field which is 120 Gauss. K is set as 1.5. Since the direction of the biasing field is parallel to the thin film, the demagnetization factors are set as $N_x = 0, N_y = 1\ and\ N_z = 0$. So the resonance frequency is given by Kittel's equation:

$$\omega_r = \sqrt{(\omega_0 + \omega_m N_x)(\omega_0 + \omega_m N_y)} = \sqrt{\omega_0(\omega_0 + \omega_m)} \approx 3.5\text{GHz} \qquad (4.1)$$

, which is consistent with the measured result. Then the damping factor α is calculated as 0.0129. The Linewidth ΔH can be calculated as about 45 Gauss.

4.2 Laminated FeGaB

Figure 4.4 and Figure 4.5 show the real part and imaginary part of the relative permeability in frequency-field spectra extracted from the measurements of Laminated FeGaB. FMR can be observed in both parts of the complex relative permeability. And resonance frequency moves from the lower band to the higher band, as the strength of the magnetic biasing field increases. K is set as 0.8 for FeGaB.

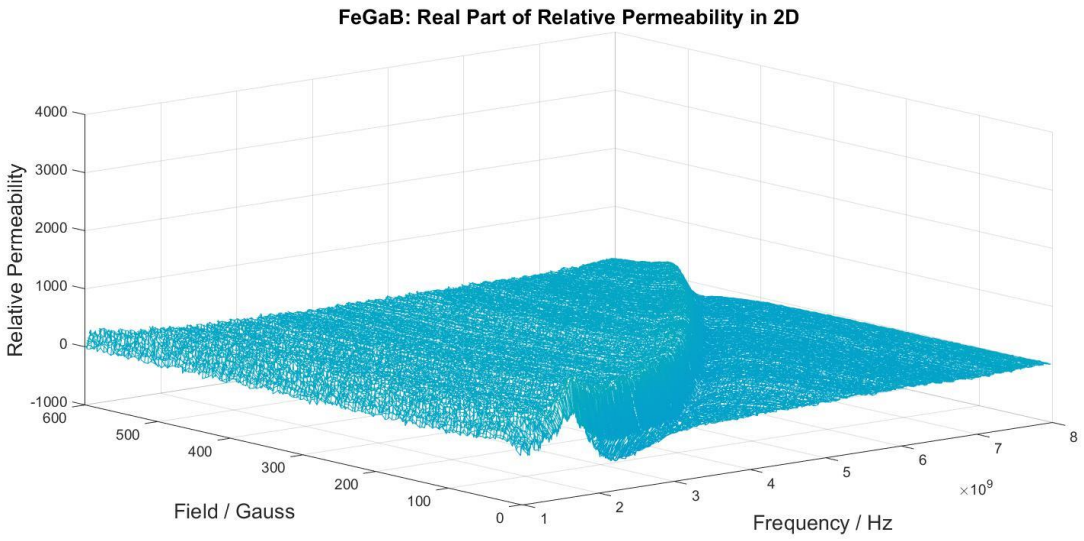

Fig. 4.4 μ_r' of laminated FeGaB in the field-frequency spectra

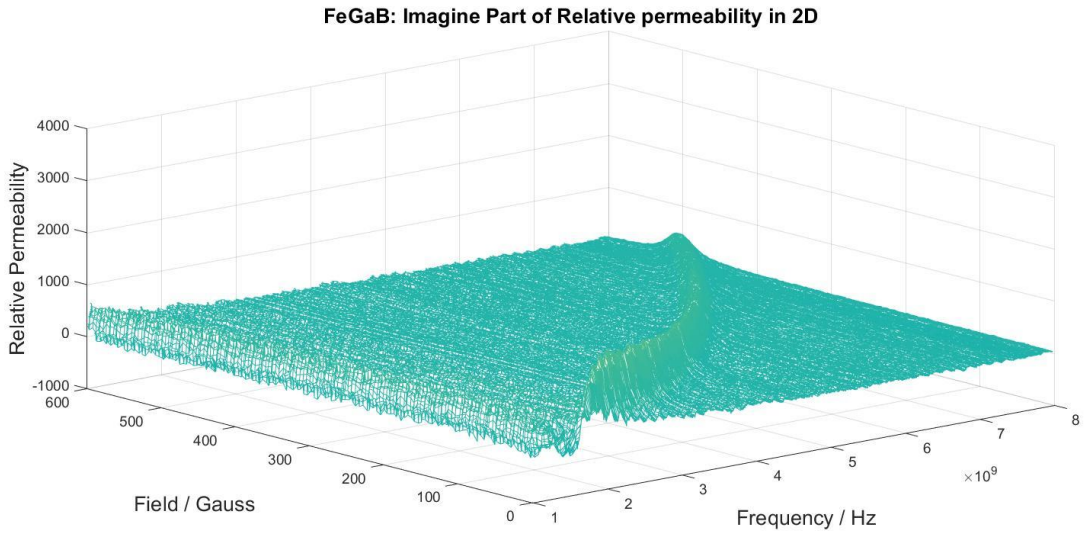

Fig. 4.5 μ_r'' of laminated FeGaB in the field-frequency spectra

Figure 4.6 shows the complex permeability in only frequency spectra at certain magnetic biasing field which is 103 Gauss. Since the direction of the biasing field is parallel to the thin film, the demagnetization factors are set as $N_x = 0, N_y = 1\ and\ N_z = 0$. So the resonance frequency is given by Kittel's equation:

$$\omega_r = \sqrt{(\omega_0 + \omega_m N_x)(\omega_0 + \omega_m N_y)} = \sqrt{\omega_0(\omega_0 + \omega_m)} \approx 3\text{GHz} \qquad (4.2)$$

, which is consistent with the measured result.

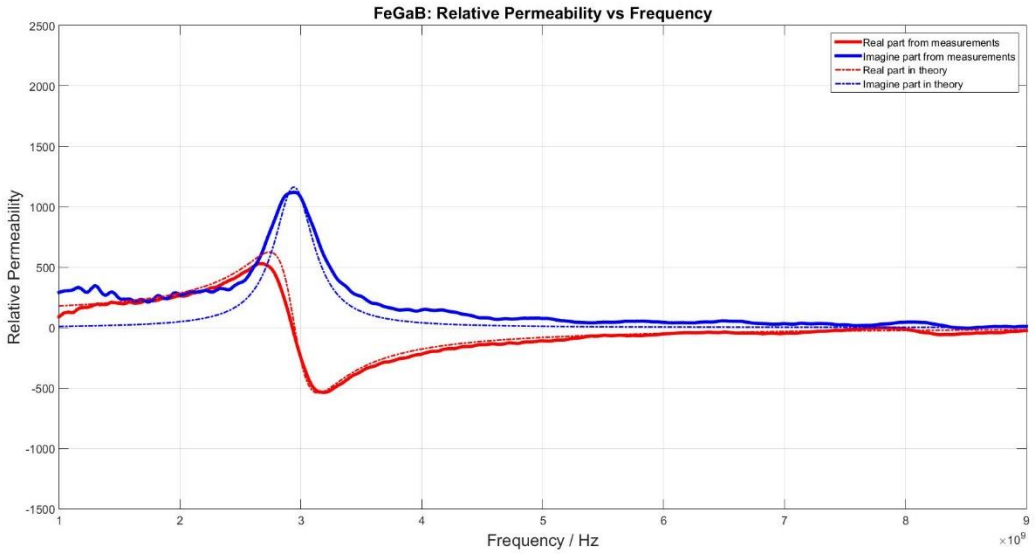

Fig. 4.6 μ_r' and μ_r'' of laminated FeGaB in frequency spectra compared with theoretical results

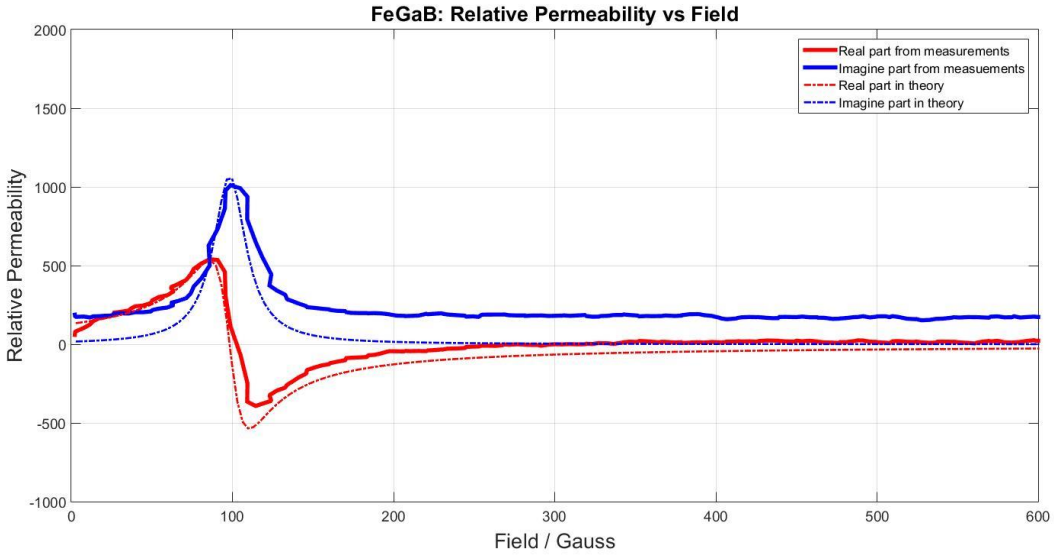

Fig. 4.7 μ_r' and μ_r'' of laminated FeGaB in field spectra compared with theoretical results

Figure 4.7 shows the complex permeability in only field spectra at resonance frequency which is 3GHz. The FMR is observed when the biasing field reaches 103Gauss, which agrees with Figure 4.6. The Linewidth ΔH can be extracted directly from Figure 4.6, which is approximately 37.5 Gauss. Then the damping factor α is calculated as 0.0107.

In Figure 4.8 and Figure 4.9, complex permeability with different biasing fields and various resonance frequencies are compared. The value of real part of the relative permeability will decrease when the resonance frequency moves to the higher band. And the linewidth will enlarge dynamically.

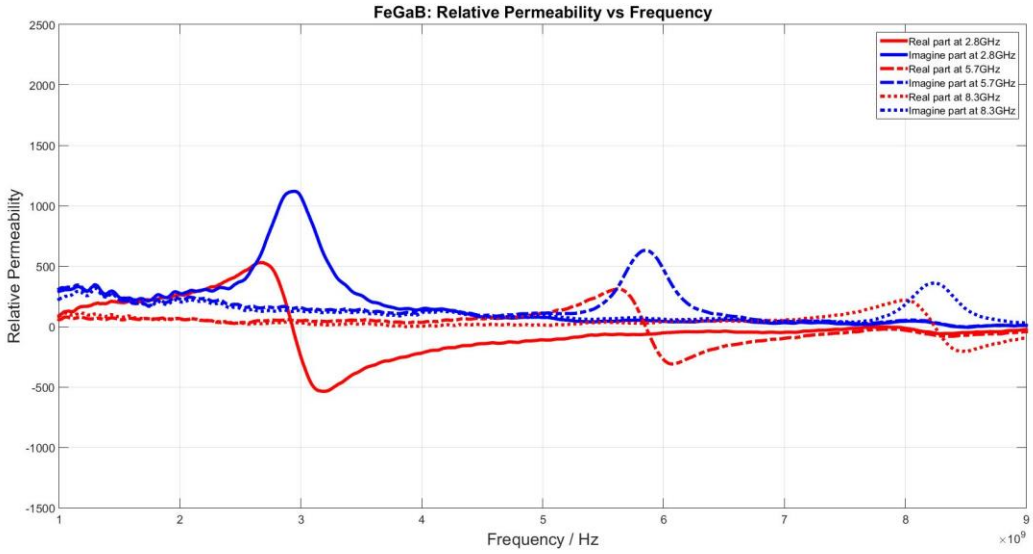

Fig. 4.8 Lam FeGaB μ at 2.8GHz-91.04Gauss, 5.7GHz-262.41Gauss and 8.3GHz-459.78Gauss

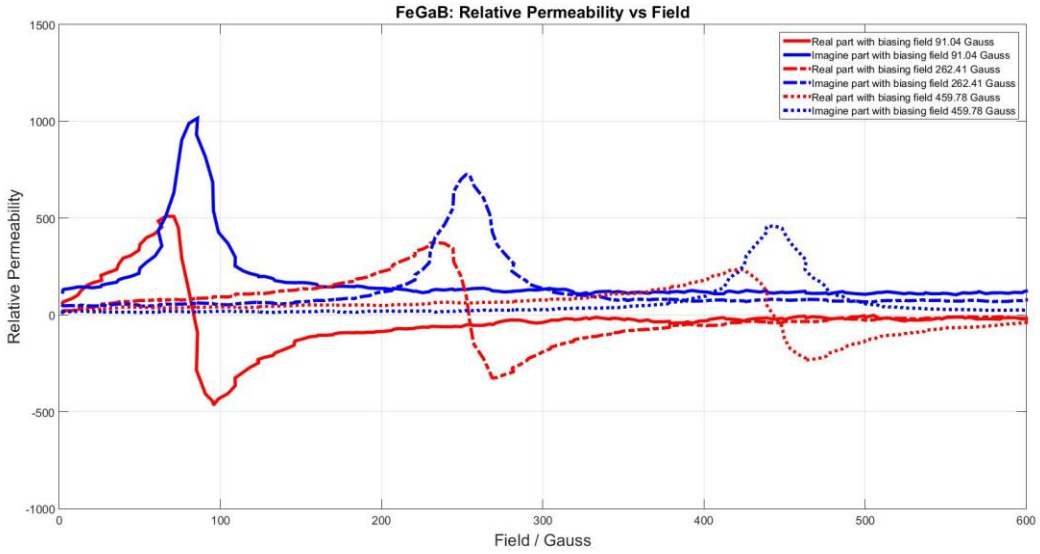

Fig. 4.9 Lam FeGaB μ at 91.04Gauss-2.8GHz, 262.41Gauss-5.7GHz and 459.78Gauss-8.3GHz

Figure 4.10 and Figure 4.11 shows the comparison between the results of continuous FeGaB and laminated FeGaB. Since the eddy current induced inside the thin film is broken by multilayers of lamination. The loss caused by eddy current will decrease, which results in smaller linewidth of laminated FeGaB than continuous FeGaB for roughly 8 Gauss in difference.

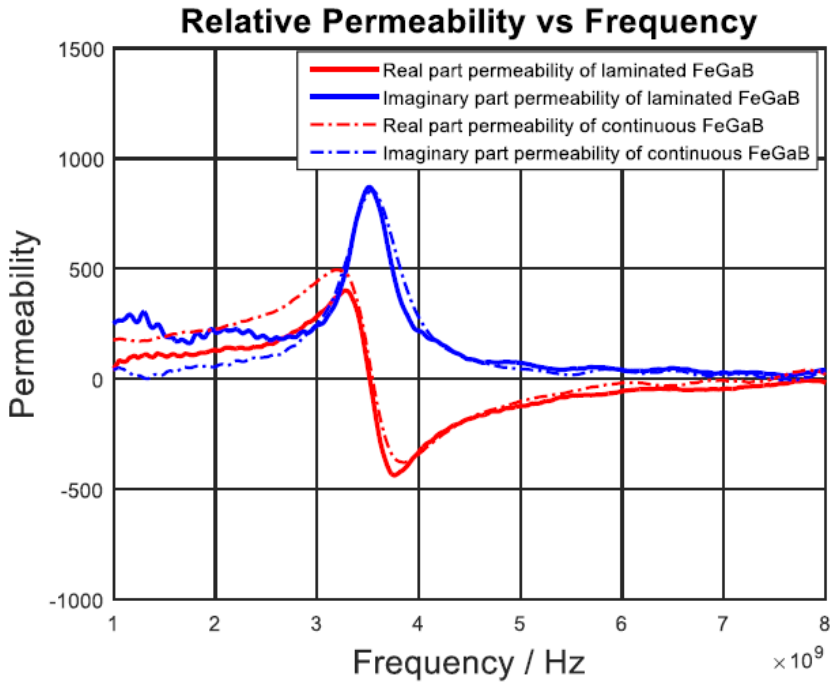

Fig. 4.10 Comparison of μ between continuous and laminated FeGaB in frequency spectra

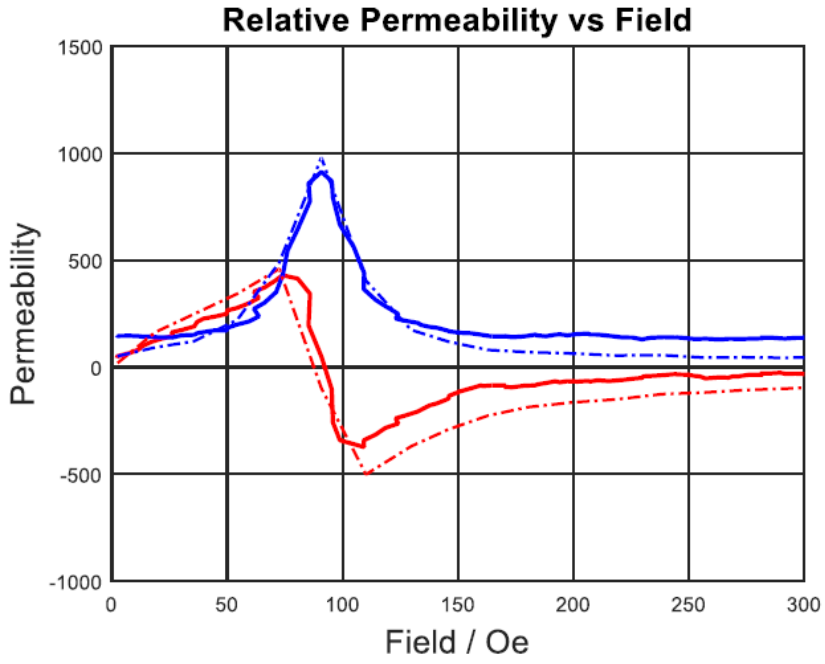

Fig. 4.11 Comparison of μ between continuous and laminated FeGaB in field spectra

4.3 NiFe

Figure 4.12 to 4.15 show the measured and theoretical results of the relative permeability of NiFe in frequency-field spectra. All the results for NiFe are induced under the condition that K is set as 1.09. FMR can be observed at 3.5GHz when the strength of the biasing field reaches 93Gauss. Linewidth is read from Figure 4.15 as 40 Gauss, which is close to 30 Gauss obtained in Squid Experiment.

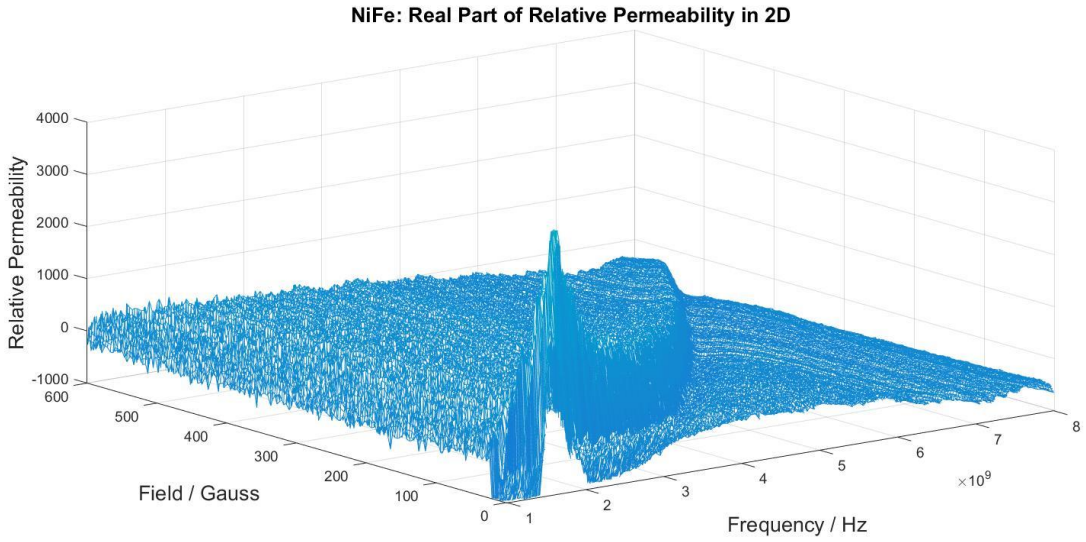

Fig. 4.12 μ_r' of NiFe in the field-frequency spectra

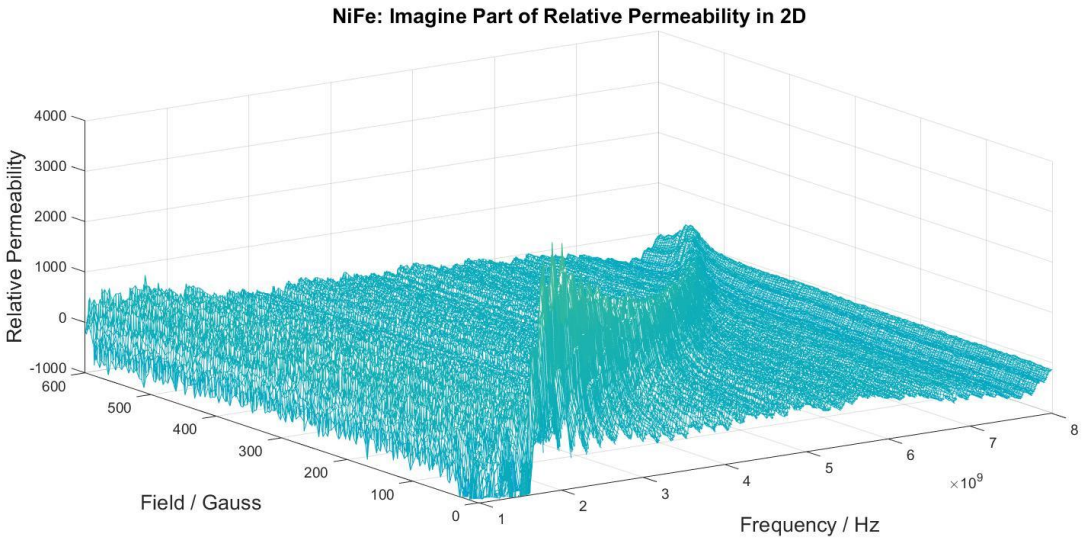

Fig. 4.13 μ_r'' of NiFe in the field-frequency spectra

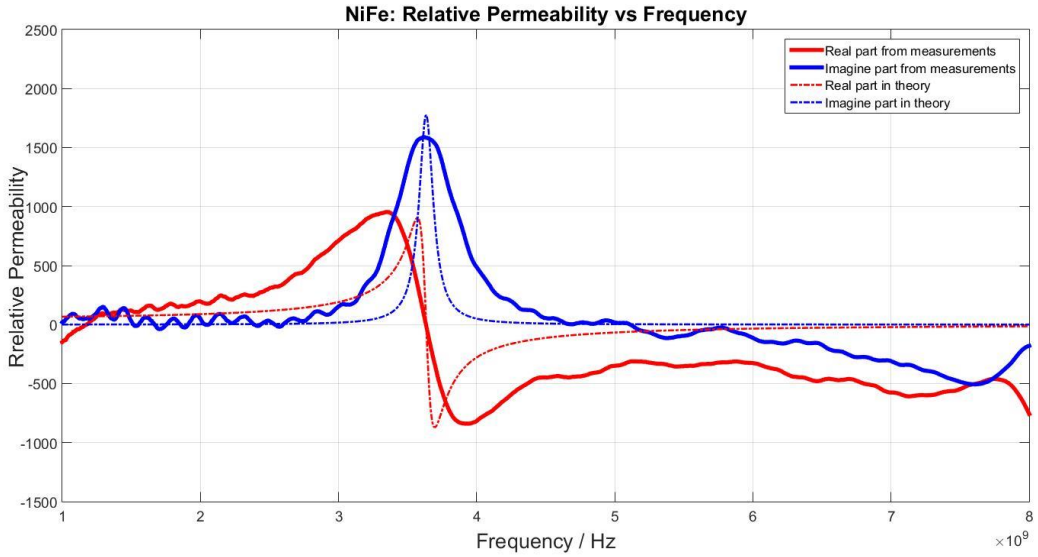

Fig. 4.14 μ_r' and μ_r'' of NiFe in frequency spectra compared with theoretical results

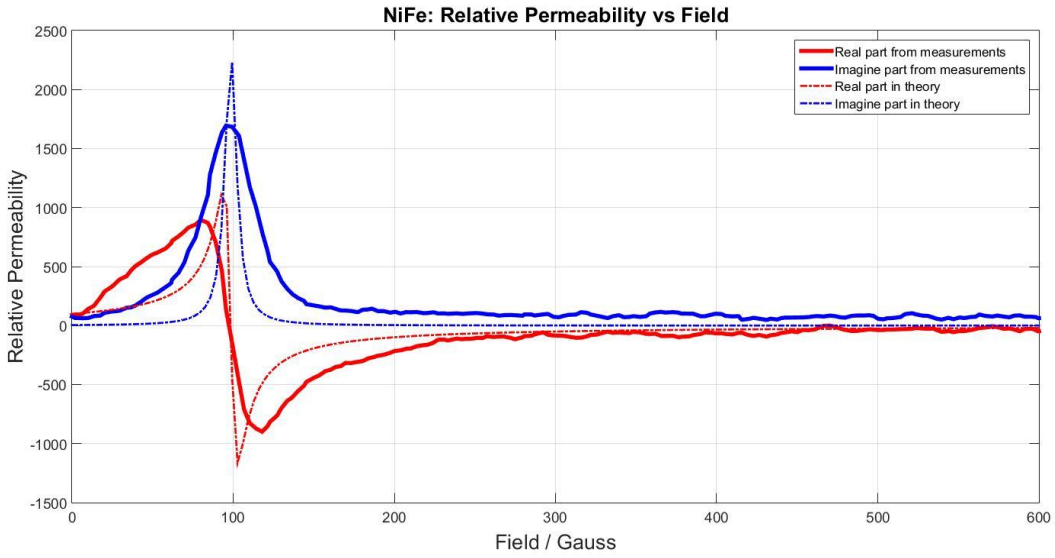

Fig. 4.15 μ_r' and μ_r'' of NiFe in field spectra compared with theoretical results

CHAPTER 5

Conclusion

5.1 Summary

A broadband dynamic characterization technique for thin film magnetic material in the field-frequency spectra is presented. The design of the strip line testbed with housing is shown. The automatic control measurement setup is narrated in detail. An improving adaptive de-embedding method is developed. The complex relative permeability and linewidth of continuous FeGaB, laminated FeGaB and NiFe are deduced from the measurements. The validity of the approach is assessed by comparing to the theoretical model.

APPENDIX A

The Matlab Code for Measured and Theoretical Permeability Calculation

```
clc
clear all
close all

% For Sample of Laminated FeGaB
% The maximum current to drive the magnet is 5A

% Parameter Definition
i = sqrt(-1);
c0 = 3*10^8; % the speed of the light
K=0.8; % Scaling factor *need to be adjusted accordingly*
thickness_d=350*10^(-9); % 330nm *need to be adjusted accordingly*
h=1*10^(-3);
l1=0*10^(-3);  % 10^(-3) unit:mm
l2=5*10^(-3); % length of sample *need to be adjusted accordingly*
l3=5*10^(-3);
l_sample=l2;
l_empty=l1+l3;
N=1601; %Frequency sweep points
M=188; %Field sweep points

% Read datas

filename = 'LAM_FEGAB_L1_L_MID_FWD_MAG.DAT';
delimiterIn = ',';
Mag_L = importdata(filename,delimiterIn);

filename = 'LAM_FEGAB_L1_L_MID_FWD_PHA.DAT';
delimiterIn = ',';
Pha_L = importdata(filename,delimiterIn);

filename = 'LAM_FEGAB_L1_T_MID_FWD_MAG.DAT';
delimiterIn = ',';
```

```
Mag_T = importdata(filename,delimiterIn);

filename = 'LAM_FEGAB_L1_T_MID_FWD_PHA.DAT';
delimiterIn = ',';
Pha_T = importdata(filename,delimiterIn);

filename = 'NEW_ALL_EMPTY_HOUSING_L_FWD_MAG.DAT';
delimiterIn = ',';
Mag_L_empty = importdata(filename,delimiterIn);

filename = 'NEW_ALL_EMPTY_HOUSING_L_FWD_PHA.DAT';
delimiterIn = ',';
Pha_L_empty = importdata(filename,delimiterIn);

filename = 'NEW_ALL_EMPTY_HOUSING_T_FWD_MAG.DAT';
delimiterIn = ',';
Mag_T_empty = importdata(filename,delimiterIn);

filename = 'NEW_ALL_EMPTY_HOUSING_T_FWD_PHA.DAT';
delimiterIn = ',';
Pha_T_empty = importdata(filename,delimiterIn);

%Frequency and Field index stored into two different arrays for future use

Freq = zeros(N,1);
Field = zeros(1,M);
Field
=(Mag_L(1,2:(M+1))+Mag_L_empty(1,2:(M+1))+Mag_T(1,2:(M+1))+Mag_T_empty(1,2:(M+1
)))/4;
Freq = Mag_L(2:(N+1),1);
Omega=2*pi*repmat(Mag_L(2:(N+1),1),1,M);
Gamma_air=(i*2*pi*repmat(Freq,1,M)/c0);

%Recover the measurements in 3D figure

figure();
%Plot the Mag_L
mesh(Freq,Field,Mag_L(2:N+1,2:M+1).');
xlabel('Frequency / Hz','FontSize',20);
ylabel('Field / Oe','FontSize',20);
zlabel('Power Ratio / dB','FontSize',20);
title('S11 with Longitudinal Bias','FontSize',20);

figure();
%Plot the Mag_T_empty
mesh(Freq,Mag_T_empty(1,2:M+1),Mag_T_empty(2:N+1,2:M+1).');
```

```
xlabel('Frequency / Hz','FontSize',20);
ylabel('Field / Oe','FontSize',20);
zlabel('Power Ratio / dB','FontSize',20);
title('S11 with Transverse Bias and Empty Housing','FontSize',20);

%Transfer the data from magnitude and phase form to real and imagine form and restore them in new matrix
%Deembedding the S11

S11_T_empty=zeros(N,M);
Mag_T_empty_de=zeros(N,M);
Pha_T_empty_de=zeros(N,M);

Mag_T_empty_de=db2mag(Mag_T_empty(2:(N+1),2:(M+1))-
repmat(Mag_T_empty(2:(N+1),(M-3)),1,M));

Pha_T_empty_de=unwrap(2*pi*Pha_T_empty(2:(N+1),2:(M+1))/360)-
unwrap(2*pi*repmat(Pha_T_empty(2:(N+1),(M-3)),1,M)/360);

S11_T_empty=Mag_T_empty_de.*exp(i*Pha_T_empty_de).*exp(-2*Gamma_air*l_sample);

S11_T=zeros(N,M);
Mag_T_de=zeros(N,M);
Pha_T_de=zeros(N,M);

Mag_T_de=db2mag(Mag_T(2:(N+1),2:(M+1))-repmat(Mag_T_empty(2:(N+1),(M-3)),1,M));

Pha_T_de=unwrap(2*pi*Pha_T(2:(N+1),2:(M+1))/360)-
unwrap(2*pi*repmat(Pha_T_empty(2:(N+1),(M-3)),1,M)/360);

S11_T=Mag_T_de.*exp(i*Pha_T_de).*exp(-2*Gamma_air*l_sample);

S11_L=zeros(N,M);
Mag_L_de=zeros(N,M);
Pha_L_de=zeros(N,M);

Mag_L_de=db2mag(Mag_L(2:(N+1),2:(M+1))-repmat(Mag_L_empty(2:(N+1),(M-3)),1,M));

Pha_L_de=unwrap(2*pi*Pha_L(2:(N+1),2:(M+1))/360)-
unwrap(2*pi*repmat(Pha_L_empty(2:(N+1),(M-3)),1,M)/360);

S11_L=Mag_L_de.*exp(i*Pha_L_de).*exp(-2*Gamma_air*l_sample);

% Calculate the permittivity and permeability

S11_empty_log=log(S11_T_empty);
```

```
S11_substrate_log=log(S11_T);

S11_film_log=log(S11_L);% ln(S11_film)

epsilon_empty=((i*c0*S11_empty_log)./(2*Omega*(l_sample+l_empty))).^2;

epsilon_substrate=((i*c0*S11_substrate_log./(2*Omega*l_sample))-
((epsilon_empty.^0.5)*l_empty/l_sample)).^2;

mu_eff=(i*c0*S11_film_log./(2*Omega.*l_sample.*(epsilon_substrate.^0.5))-
(epsilon_empty.^0.5)*l_empty./((epsilon_substrate.^0.5)*l_sample)).^2;

mu_relative=(mu_eff-1)/(K*(thickness_d/h));

mu_relative_real= repmat(zeros(N,1),1,M);
mu_relative_imag= repmat(zeros(N,1),1,M);

for k = 1: M

   mu_relative_real(1:N,k)=real(mu_relative(1:N,k));
   mu_relative_imag(1:N,k)=-imag(mu_relative(1:N,k));

end

figure();
mesh(Freq,Field,mu_relative_real.');
xlabel('Frequency / Hz','FontSize',20);
ylabel('Field / Gauss','FontSize',20);
zlabel('Relative Permeability','FontSize',20);
title('FeGaB: Real Part of Relative Permeability in 2D','FontSize',20);
axis([1*10^9 8*10^9 0 600 -1000 4000]);
hold on;
grid on;

figure();
mesh(Freq,Field,mu_relative_imag.');
xlabel('Frequency / Hz','FontSize',20);
ylabel('Field / Gauss','FontSize',20);
zlabel('Relative Permeability','FontSize',20);
title('FeGaB: Imagine Part of Relative permeability in 2D','FontSize',20);
axis([1*10^9 8*10^9 0 600 -1000 4000]);
hold on;
grid on;

% Theoretical Permeability Calculation based on Kittel's Equations in 2D
```

```
EP0=8.84e-12; % Epsilon, free space permittivity
MU0=4.0*pi*1.0E-7; %Mu, free space permeability
CC=3.0*1.e8; %Speed of light in free space
f_s=1e9; %Frequency of the wave, if sinusoidal excitation is used
gamma=-1.759*10^11; % Unit is C/kg
Hi=[3.4200:(624.8000-3.4200)/(M-1):624.8000]/(4*pi*10^-3); % unit is A/m
Ms=(800*4*pi)/(4*pi*10^-3); % unit is tesla, NiFe=800 emu/cc
delta_H=30; %line width in the unit of Oesterd
freq=[50*10^6:(10*10^9-50*10^6)/(N-1):10*10^9];
freq=freq.';

% Calculation of the theoretical permeability

Wm=2*pi*2.8e6*Ms*4*pi*1.e-3;  %Saturation magnetization
W0_0=repmat(2*pi*2.8e6*Hi*4*pi*1.e-3,N,1);
W=repmat(2*pi*freq,1,M);   %Angular Frequency
Wr=sqrt(W0_0.*(Wm+W0_0));
alpha=-delta_H*2.8e6/9.8e9/2; %damping constant
W0=W0_0+i*alpha*W; %Complex FMR of bulk due to damping
su_complex=Wm.*(Wm+W0)./(W0.*(Wm+W0)-W.^2); %complex susceptability of the film

mu_p= repmat(zeros(N,1),1,M);
mu_d= repmat(zeros(N,1),1,M);
for g = 1: M
mu_p(1:N,g)=1+real(su_complex(1:N,g)); %real part of the permeability
mu_d(1:N,g)=imag(su_complex(1:N,g)); %imaginary part of the permeability
end


figure();
mesh(freq,Hi*(4*pi*10^-3),mu_p.');
hold on;
% axis([1*10^9 8*10^9 0 600 -3500 6000]);
xlabel('Frequency / Hz','FontSize',20);
ylabel('Field / Gauss','FontSize',20);
zlabel('Relative Permeability','FontSize',20);
title('FeGaB: Real Part of Relative Permeability in 2D','FontSize',20);
grid on;

figure();
mesh(freq,Hi*(4*pi*10^-3),mu_d.');
hold on;
% axis([1*10^9 8*10^9 0 600 -500 6000]);
xlabel('Frequency / Hz','FontSize',20);
ylabel('Field / Gauss','FontSize',20);
```

```
zlabel('Relative Permeability','FontSize',20);
title('FeGaB: Imagine Part of Relative Permeability in 2D','FontSize',20);
grid on;

% Check the real part and imagine part of permeability for certain bias field over whole scale of
frequency

% Plot both the real and imagine part of the permeability

figure();
plot(Freq,smooth(mu_relative_real(1:N,17),50),'r','LineWidth',4);
hold on;
plot(Freq,smooth(mu_relative_imag(1:N,17),50),'b','LineWidth',4);
xlabel('Frequency / Hz','FontSize',20);
ylabel('Relative Permeability','FontSize',20);
title('FeGaB: Relative Permeability vs Frequency','FontSize',20);
axis([1*10^9 8*10^9 -1000 2500]);
grid on;

% Theoretical permeability calculation based on Kittel's equation in 1D (Permeability vs
Frequency)

% Parameter Definition (ought to be changed)

EP0=8.84e-12; % Epsilon, free space permittivity
MU0=4.0*pi*1.0E-7; %Mu, free space permeability
CC=3.0*1.e8; %Speed of light in free space
f_s=1e9; %Frequency of the wave, if sinusoidal excitation is used
gamma=-1.759*10^11; % Unit is C/kg
Hi=83.55/(4*pi*10^-3); % unit is A/m
Ms=(1050*4*pi)/(4*pi*10^-3); % unit is A/m, NiFe=800 emu/cc
delta_H=75; %line width in the unit of Oesterd
f=[50*10^6:(10*10^9-50*10^6)/(N-1):10*10^9];

% Calculation of the theoretical permeability

Wm=2*pi*2.8e6*Ms*4*pi*1.e-3;  %Saturation magnetization
W0_0=2*pi*2.8e6*Hi*4*pi*1.e-3;
W=2*pi*f;   %Angular Frequency
Wr=sqrt(W0_0*(Wm+W0_0));
alpha=-delta_H*2.8e6/9.8e9/2; %damping constant
W0=W0_0+i*alpha*W; %Complex FMR of bulk due to damping
su_complex=Wm*(Wm+W0)./(W0.*(Wm+W0)-W.^2); %complex susceptability of the film
mu_p=1+real(su_complex); %real part of the permeability
mu_d=imag(su_complex); %imaginary part of the permeability
```

```
figure();
plot(Freq,smooth(mu_relative_real(1:N,17),50),'r','LineWidth',4);
hold on;
plot(Freq,smooth(mu_relative_imag(1:N,17),50),'b','LineWidth',4);
hold on;
plot(f,mu_p,'y','LineWidth',2);
hold on;
plot(f,mu_d,'g','LineWidth',2);
hold on;
xlabel('Frequency / Hz','FontSize',20);
ylabel('Relative Permeability','FontSize',20);
title('FeGaB: Relative Permeability vs Frequency','FontSize',20);
axis([1*10^9 9*10^9 -1500 2500]);
grid on;

figure();
plot(Freq,smooth(mu_relative_real(1:N,17),50),'r','LineWidth',4);
hold on;
plot(Freq,smooth(mu_relative_imag(1:N,17),50),'b','LineWidth',4);
hold on;
plot(Freq,smooth(mu_relative_real(1:N,80),50),'-.r','LineWidth',4);
hold on;
plot(Freq,smooth(mu_relative_imag(1:N,80),50),'-.b','LineWidth',4);
hold on;
plot(Freq,smooth(mu_relative_real(1:N,160),50),':r','LineWidth',4);
hold on;
plot(Freq,smooth(mu_relative_imag(1:N,160),50),':b','LineWidth',4);
hold on;
% plot(f,mu_p,'y','LineWidth',2);
% hold on;
% plot(f,mu_d,'g','LineWidth',2);
% hold on;
xlabel('Frequency / Hz','FontSize',20);
ylabel('Relative Permeability','FontSize',20);
title('FeGaB: Relative Permeability vs Frequency','FontSize',20);
axis([1*10^9 9*10^9 -1500 2500]);
grid on;

% Check the real part and imagine part of permeability for certain frequency over whole scale of
bias filed

figure();
plot(Field,-smooth(mu_relative_real(550,1:M),5),'r','LineWidth',4);
hold on;
plot(Field,smooth(mu_relative_imag(550,1:M),5),'b','LineWidth',4);
hold on;
```

```
plot(Field,-smooth(mu_relative_real(912,1:M),5),'-.r','LineWidth',4);
hold on;
plot(Field,smooth(mu_relative_imag(912,1:M),5),'-.b','LineWidth',4);
hold on;
plot(Field,-smooth(mu_relative_real(1200,1:M),5),':r','LineWidth',4);
hold on;
plot(Field,smooth(mu_relative_imag(1200,1:M),5),':b','LineWidth',4);
hold on;
xlabel('Field / Gauss','FontSize',20);
ylabel('Relative Permeability','FontSize',20);
title('FeGaB: Relative Permeability vs Field','FontSize',20);
axis([0 600 -1000 1500]);
grid on;

% Theoretical permeability calculation based on Kittel's equation in 1D (Permeability vs Field)
% Parameter Definition (ought to be changed)

EP0=8.84e-12; % Epsilon, free space permittivity
MU0=4.0*pi*1.0E-7; %Mu, free space permeability
CC=3.0*1.e8; %Speed of light in free space
f_s=1e9; %Frequency of the wave, if sinusoidal excitation is used
gamma=-1.759*10^11; % Unit is C/kg
Hi=[3.4200:(624.8000-3.4200)/(M-1):624.8000]/(4*pi*10^-3); % unit is A/m
Ms=(1050*4*pi)/(4*pi*10^-3); % unit is A/m, NiFe=800 emu/cc
delta_H=75; %line width in the unit of Oesterd
f=3.2*10^9;%unit is Hz

% Calculation of the theoretical permeability

Wm=2*pi*2.8e6*Ms*4*pi*1.e-3; %Saturation magnetization
W0_0=2*pi*2.8e6*Hi*4*pi*1.e-3;
W=2*pi*f; %Angular Frequency
Wr=sqrt(W0_0.*(Wm+W0_0));
alpha=-delta_H*2.8e6/9.8e9/2; %damping constant
W0=W0_0+i*alpha*W; %Complex FMR of bulk due to damping
su_complex=Wm*(Wm+W0)./(W0.*(Wm+W0)-W.^2); %complex susceptability of the film
mu_p=1+real(su_complex); %real part of the permeability
mu_d=imag(su_complex); %imaginary part of the permeability

figure();
plot(Field,-smooth(mu_relative_real(600,1:M),5),'r','LineWidth',4);
hold on;
plot(Field,smooth(mu_relative_imag(600,1:M),5),'b','LineWidth',4);
hold on;
plot(Hi*(4*pi*10^-3),-mu_p,'-.r','LineWidth',2);
hold on;
```

```
plot(Hi*(4*pi*10^-3),mu_d,'-.b','LineWidth',2);
hold on;
xlabel('Field / Gauss','FontSize',20);
ylabel('Relative Permeability','FontSize',20);
title('FeGaB: Relative Permeability vs Field','FontSize',20);
axis([0 600 -1000 2000]);
grid on;
```

REFERENCES

[1] V. Bekker, K. Seemann, H. Leiste, "A new strip line broad-band measurement evaluation for determining the complex permeability of thin ferromagnetic films." Journal of Magnetism and Magnetic Materials, vol. 270, issue 3, pp. 327-332, April 2004.

[2] Y. Liu "Broadband complex permeability characterization of magnetic thin films using shorted microstrip transmission-line perturbation, " Rev. Sci. Instrum., 76, 063911, 2005.

[3] Lepetit, T., Neige, J., Adenot-Engelvin, A.L. Ledieu, M., "Accurate Characterization of both Thin and Thick Magnetic Films Using a Shorted Microstrip." , Magnetics, IEEE Transactions on, vol. PP, issue 99, pp: 1-1, 2014.

[4] David M. Pozar “Microwae Engineering, 4th edition”, John Wiley & Sons, Inc, Copyright 2012, ISBN: 978-0-470-63155-3

[5] C.A. Grimes, J.V. Prodan, J. Appl. Phys. 73 (1993) 6989.

[6] M. Yamaguchi, S. Yabukami, K.I. Arai, IEEE Trans. Magn. 33(5) (1997) 4044

[7] Z. Yao, Y. Wang, S. Kellor and G. Carman, “Bulk Acoustic Wave Mediated Multiferroic Antennas Architecture and Performance Bound”, IEEE Trans. Antenna and Propagation, Vol 63

[8] D. Pain, et al., J.Appl. Phys. 85(1999) 5151.